SAND2020-10662C

LiDAR For Heliostat Optical Error Assessment

Charles Q. Little[1, a)], Daniel E. Small[3, b)], Julius Yellowhair[3, c)]

[1, 2]*Sandia National Laboratories, P.O. Box 5800, Albuquerque, NM 87185 USA.*
[3]*Gryphon Technologies, 2309 Renard Pl SE #120, Albuquerque, NM 87131 USA.*

[a)] cqlittl@sandia.gov
[b)] desmall@sandia.gov
[c)] jey422@gmail.com

Abstract. This project extends our experience in **Li**ght **D**etection **A**nd **R**anging (LiDAR) to gain an understanding of the abilities and limits of using 3D laser scanning to capture the relative canting angles between heliostat mirror surfaces in 3-space to an accuracy sufficient to measure canting errors. As far as we are aware, this approach has never been developed or implemented for this purpose. The goal is to be able to automatically perform a 3D scan, retrieve the data, and use computational geometry and a-priori mechanical knowledge of the heliostats (facet arrangement and size) to filter and isolate the facets, and fit planar models to the facet surfaces. We currently use FARO Focus 3D laser range scanners which provide a dense data coverage of the scan area in the form of a 3D point cloud. Each point has the 3D coordinates of the surface position illuminated by the device as it scans the laser beam over an area, both in azimuth and elevation. These scans can contain millions of points in total. Our initial plan was to primarily use the back side of the heliostat to capture the mirror (the back side being opaque). We did not expect to capture high-quality data from the reflective front side. We were surprised by the discovery that the front side did, indeed, yield surface data. This is a function of the soiling, or collected dust, on the mirror surface. We are seeing typical point counts on the mirror facets of between 10k – 100k points per facet, depending on the facet area and the scan point density. By collecting facet surface points, the data can be used to calculate an individual planar fit per facet, the normals of which correlate directly with the facet pointing angle. Comparisons with neighboring facets yield the canting angles. Our process includes software which automatically: 1) controls the LiDAR scanner and downloads the resultant scan data, 2) isolates the heliostat data from the full scan, 3) filters the points associated with each individual facet, and 4) calculates the planar fit and relative canting angles for each facet. This goal of this work has been to develop this system to measure heliostat canting errors to < 0.25 mrad accuracy, in a time under 5 minutes per heliostat. A future goal is to place this or a comparable sensor on an autonomous platform, along with the software system, to collect and analyze heliostats in the field for tracking and canting errors in real time. This work complements Sandia's strategic thrust in autonomy for CSP collector systems

INTRODUCTION

Sandia Labs has had a long-standing role in research and development of solar energy systems; in particular, concentrated solar power technology, with heliostats outfitted with multiple facets targeting sunlight at a target on a central tower. Figure 1 (left) shows the Sandia National Laboratories National Solar Thermal Test Facility (NSTTF) solar tower and heliostat field located in Albuquerque, New Mexico, USA. Figure 1 (right) shows a single heliostat in that field. Clearly, the performance of the heliostat field can be impacted by mirror canting errors, tracking errors, and soiling. Each of these issues will reduce the sunlight hitting the target and therefore the performance of the field.

Figure 1 Sandia NSTTF solar tower and the heliostat field (left) and an NSTTF heliostat with 3D LiDAR Scanner

Sandia has in the past and continues to develop tools for heliostat focusing and canting enhancement (HFACET) [1 - 2]. In regard to a current project (UFACET) [3], we were asked to see if LiDAR scanning could be used to locate the position of a facet in 3D, mostly as a test to acquire truth data. The conventional wisdom says LiDAR scanning does not work well on reflective surfaces. So, we proposed putting checkerboard targets on the corners of the facets. We have software that can automatically find checkerboard targets, and this would give us a simple way to capture four points on the facet and use those to calculate the plane of the facet. The normal to the plane would give us the pointing angle. The position and normal of multiple facets on a heliostat would provide the data to calculate the canting angles. We tested the targets at 10 meters, and then went to the field and placed them on the heliostat facet corners. Our experiment worked better than expected. Figure 2 shows the checkboard target, the resulting LiDAR scan data in the lab at 10 meters, and the resulting LiDAR scan data of the targets placed on the facet corners of a heliostat.

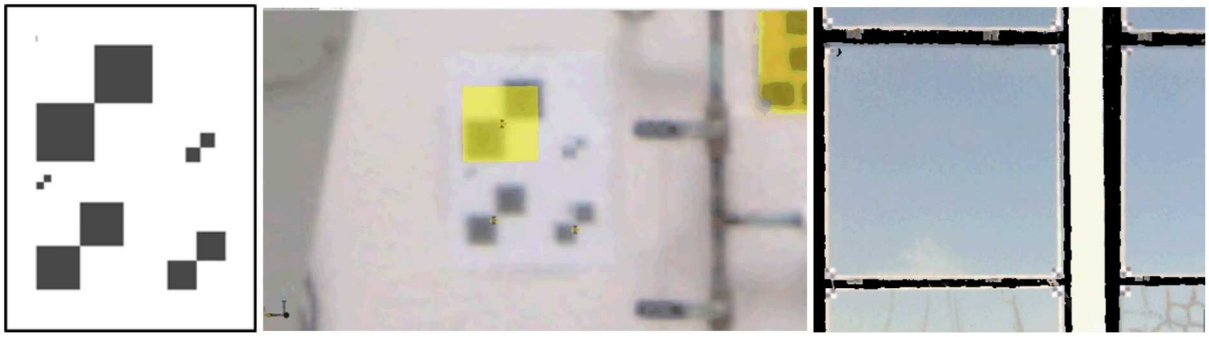

Figure 2. Checkerboard; target, scan results on wall at 10 meters, scan result on heliostat facet in field.

As seen in the Figure 2, the mirror surface is manifestly visible in the scan data. This was a ‘eureka’ moment. It meant we did not need the checkerboard target at all. We could use the entire surface of the facet to know its location relative to its neighbors as well as fit a plane to find its pointing angle. The rest of this paper describes how.

LIDAR SCANNING OF HELIOSTATS

A LiDAR scanner uses a laser to detect the distance from the scanner to objects in its surroundings. The technology used is time-of-flight (or phase shift). These scanners typically are mounted on a stationary platform, like a tripod, to maintain a fixed position while scanning. (They can be mounted on moving platforms, but that requires additional localization hardware to combine the data to a single coordinate frame). While the base of the scanner is fixed, the unit itself uses a rotating mirror to scan vertically and turns the unit to scan horizontally. In this way, data can be captured of an entire area; 360 degrees horizontally and near that (minus the mounting for ~300 degrees) vertically. Range resolution is typically around ± 2mm. Practical range measurements can be read from ½ to 50 meters or more. The output is a series of locations or points in space. These points come from the reflection of the laser on the surfaces

seen by the sensor. Location here refers to the x-y-z coordinate position of the point relative to the scanner. Most surfaces will adequately reflect laser light, but not all; very shiny and non-reflective surfaces (coating, black matte) and no surface (open sky and out of range) will have false returns or no return at all. Data consists of values per point: x-y-z position and usually a laser return intensity. In addition, many 3D scanners are co-equipped with visual cameras, and can acquire color (RGB) values for each point. It is not unusual for the output to contain tens to hundreds of million points per scan. Scan times vary with point density, but a typical 50 million point scan can take < 5 minutes.

FARO 3D Scanner

For our project, we used a FARO Focus 3D [4], as shown in Figure 3. This unit weighs 10 pounds. With a 45-million-point scan, the corresponding point spacing is 6 mm at 10 meters.

Figure 3. FARO Focus3D scanner.

Mirror Surface Results

As mentioned in the introduction were very surprised to discover that in addition to the checkerboard targets, the mirror surface was also detected by the LiDAR scanner. Figure 4 is a full image of the scan data. Figure 6 is a photo image from the same heliostat. We found that mirrors with near reflections of background objects did not return the surface but instead returned the distance to the objects in reflection. Note the area where the heliostat in front of this one is reflected in the in the lower center facets. Note also the upper mirror surfaces are present; these have sky reflected in them. For further detail, Figure 5 shows a closeup of the scan data (this is from the lower left corner of the center facet). Note the density of the data.

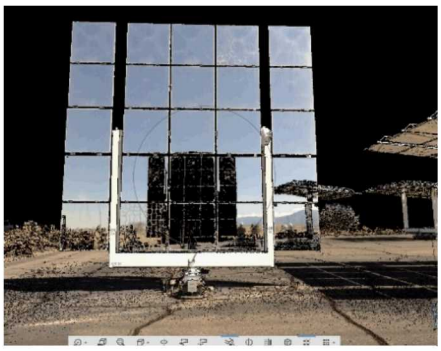
Figure 4. Full LiDAR scan of heliostat.


Figure 5. Closeup of Figure 4


Figure 6. Photo of heliostat in Figure 4


Figure 7. Heliostat scan with partially clean facet on bottom row.

Soiled versus Clean Surfaces

We believed the scanner was picking up data from the dust or soiling on the mirror surface. The test this theory, we wiped down half of one of the facets of a heliostat and scanned it. Figure 7 is the result. It is even obvious we did not clean it very well. Close visual inspection also showed most of the mirrors had a dust layer.

When we first made this proposal, it was based on taking data of a few heliostats at the National Solar Thermal Test Facility at Sandia which returned dense point clouds off the mirror surfaces remarkably well. At the time, we believed that the normal accumulation of dust on the mirror surface was enough to generate good returns. We did not realize how this might be a problem until

the mid-fall of 2019 when NSTTF staff used a common technique to clean all the mirrors simultaneously. This involves waiting for the right kind of weather; a snowstorm of 4 to 6 inches was forecast. As the storm began, the mirrors were oriented to face the sky. After snow accumulated on the horizontal heliostats, they were tilted in elevation to allow the snow to rapidly slide off the mirrors, taking away months of accumulated soiling and dust with it. This resulted in mirrors that were very clean across the entire field. Figure 8 shows the results of scanning these clean mirrors. As seen from the images, clean mirrors (seen on the left) do not scan anywhere near as well as soiled ones (seen on the right). The NSTTF heliostat design stows the mirrors upside down, which we believe is unique in large solar fields. This means that dust will take longer to adhere to the mirror surface.

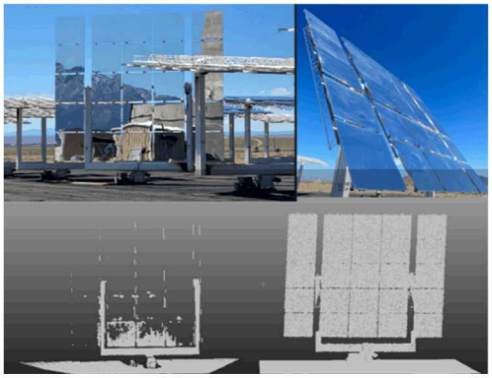

Figure 8. Clean vs. Soiled Heliostats

Since clean mirrors could pose a major limitation to our system, we successfully experimented with artificially soiling the mirrors by spraying a light cornstarch and water mixture on the heliostat. This artificial soil can be easily washed off. The facets on the right in Figure 8 were lightly sprayed with this mixture. We also began leaving 9 of the heliostats facing sky instead of ground for a stow position, which allowed them to accumulate dust again, and within 5-6 weeks, were able to be scanned without artificial soiling. In a commercial field, the scanning can be performed 180 degrees out of phase from the cleaning cycle which should yield measurable mirror surfaces at most times.

CANTING ANGLE ESTIMATION

Given that we can scan the facet mirror surface, we set out to find the canting angles of individual facets. We begin with a full scan of the heliostat, which usually includes the ground around it and other objects in the scan area (see Figure 9-A). Each point has an xyz value, and we can order the z values to estimate and remove the ground (see Figure 9-B). We then isolate the desired heliostat from its neighbors or other objects by using connected component analysis (also called blob detection) as shown in Figure 9-C. We assume we will know the geometry of the heliostat and use it as a template to separate the individual facets. The heliostats we have examined are laid out in a square grid with ample facet separations, so we are using only the 2D separation distances. We accomplish this by using the major axis of the isolated heliostat, using a bounding box algorithm [5] to then translate the data to the X-Y axis. This allows us to use the distance between facet layout of the heliostat to separate each facet. The facet data may contain extraneous data. This can be from the support structure that is sometimes scanned through the gaps between facets. An example is shown in Figure 9-D. It is also common for scanning edge effects to give false data. This occurs because the laser beam hitting the edge of objects has a finite dot size, and sometimes partially illuminates more than one surface as it spills over, causing a skirting effect. These bad points can be filtered out. We use two methods. The first uses the same z ordered filter used for the ground finder; the facet is translated to lie in the x-y plane, and then z ordered, with outliers above and below removed. Figure 9-E shows an example. Another method to filter the facet is to fit a plane and toss points further away from the plane. Both of these methods suppose outliers are in fact relatively far from the vast majority of the points, which are on the plane.

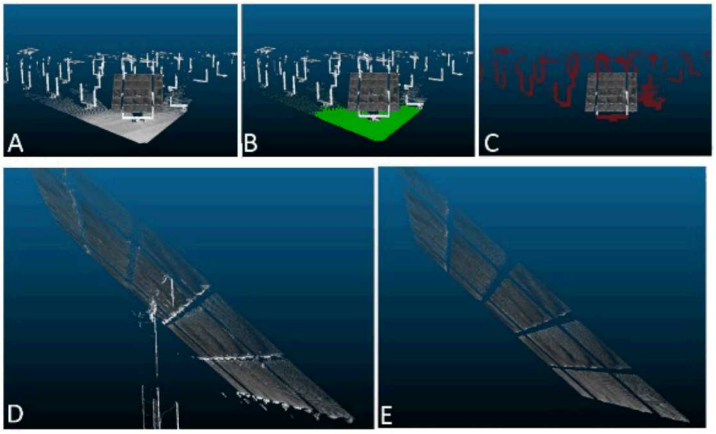

Figure 9. A - Full Heliostat Scan, B - Remove the Ground Plane, C - Remove neighboring objects, D - Filter extraneous data on all facets, E - The final filtered facet data

Finally, with clean facet information, the facet data is fit to planes. This is where the LiDAR scan brings a significant advantage in oversampling, as it can capture upwards of 100,000 points per facet. Because the +/-2mm range error is zero-mean, the planar estimate error is reduced by $\frac{1}{sqrt(N)}$ (N = total number of

points in the facet). The process subtracts the centroid of data (i.e. translating the facet points to the origin) and uses the Singular Value Decomposition method to determine the planar normal, which is used as the facet direction vector. The canting angle must be relative to something, and we pick the center facet as the control vector and compare each facet normal to the center facet normal. Figure 11 shows the segmented facets color coded. Figure 10 shows these vectors displayed from the heliostat scan, with the vector originating at the centroid of the facets. Canting angles are reported as azimuth and elevation of each plane relative to the center facet.

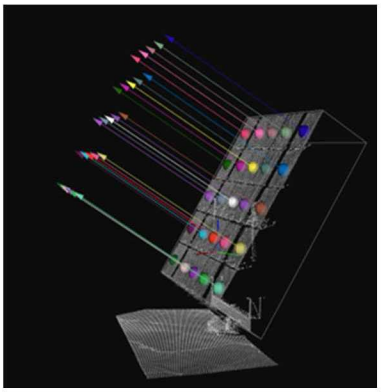

Figure 11. Canting angles shown with heliostat scan data.

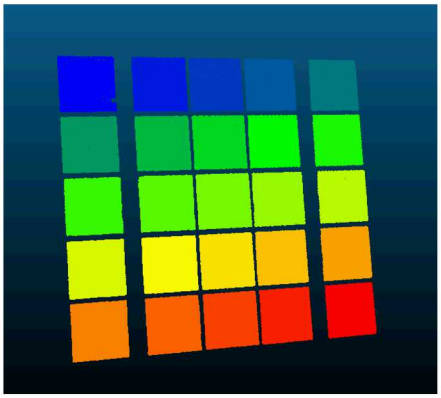

Figure 10. Automatically Segmented Facet Data

Comparison of Front Versus Back Surfaces

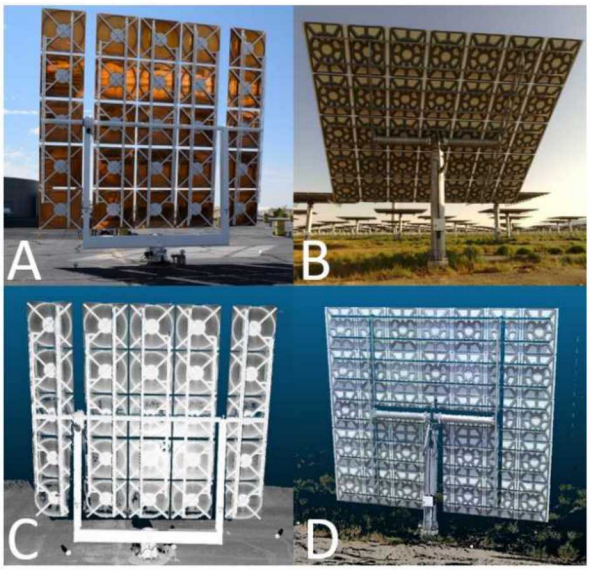

Figure 12. A - Back of NSTTF heliostat. B - Back of Crescent Dunes heliostat. C - LiDAR scan of back side, NSTTF. D - LiDAR scan of back side, Crescent Dunes.

From the beginning, we were looking to see if we could get equivalent results by scanning the back of the heliostat. On many of the heliostats we have observed, the back side has the majority of the facet visible even with the support structure. The facets themselves are composed of a glass plate, with a mirror coating on one side. To mount these plates to the heliostat structure, the NSTTF facets are glued to a steel support structure that is then bolted to the heliostat frame. Figure 12-A shows a photo of the back of an NSTTF heliostat. Figure 12-B shows the back of another heliostat design from the Crescent Dunes Solar Energy Project in Tonopah Nevada. These facets have a support frame fabricated directly onto the mirror. Both of these support structures can be seen in the point scan data, as shown in Figure 12-C and Figure 12-D respectively.

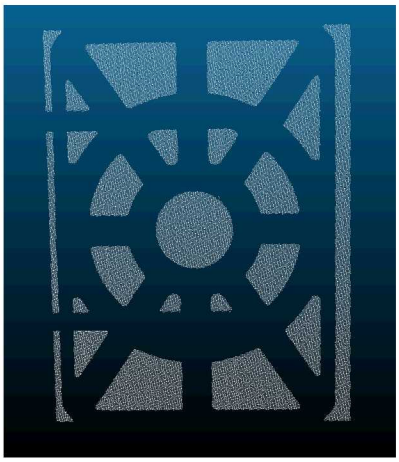

Figure 13. The filtered backside data of a Crescent Dunes facet

As seen in the images, a substantial portion of the facet is visible from the back. If this can be isolated, we should be able to use it to estimate the facet pointing direction. Unfortunately, the NSTTF back side is itself a reflective surface, and proved to be extremely noisy. However, the Crescent Dunes heliostat back side are painted white and scanned very cleanly. We were able to filter the data to remove the support structure, as shown in Figure 13.

The facet normal data for the plane should be the same for the front-side scan and back-side scan. To test this, we registered scans from the front and back for the Crescent Dunes data. Registration refers to putting the scan data into a common coordinate frame. This was done using spherical scan targets that were placed around the heliostat for both scans. The normals were expressed in azimuth and elevation as noted earlier. The comparison of front-to-back results were very favorable, with the mean errors for the 35 facets at 0.124 mrad for azimuth and 0.004 mrad for elevation. The standard deviation values were 0.98 mrad azimuth and 0.81 mrad elevation.

REPEATABILITY STUDY

A repeatability study was performed at the NSTTF which acquired more than 230 individual scans of 13 heliostats at 3 different elevation angles. Each heliostat was scanned at 3 of 4 different heliostat elevation angles; 0 degrees (vertical), 25 degrees, 30 degrees and 45 degrees. We scanned multiple (5 → 9) times at each discrete elevation angle. We then derived the relative canting angles for each scan. The standard deviation of the derived azimuth and elevation angle was calculated for each individual facet within that set of scans. We then took the RMS error of the standard deviations for each heliostat, yielding 40 discrete RMS errors in azimuth and elevation. The average RMS error in Azimuth was 0.21 mrad, and the average RMS error of Elevation was 0.20 mrad.

GRAVITATIONAL EFFECTS ON REPEATABILITY

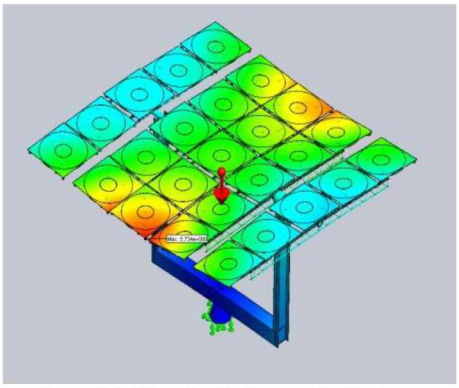

Figure 14. Gravity Deformed Heliostat in Horizontal Orientation [6]

We also have the statistics to simultaneously look at all three elevations considered in the same manner. There is an issue with comparing the relative canting angles between the same heliostat at different elevation angles, which we suggest is the deflection of the mirror facets due to gravity. In [6] the authors performed modelling that showed a maximum displacement of 5.6mm in the heliostat structure due to gravity. Simulation results from that paper are shown in Figure 14. This translates into potential displacements of 2.0 – 2.8 mrad in the canting angles. This implies that the canting angles change slightly with the elevation angle, and that the relatively tight results for RMS error in scans at the same heliostat elevation angle can be expected to change, which is consistent with the result that we found when considering the average facet RMS data for multiple elevations, which for the 13 heliostats across all elevation angles was 0.49 mrad in facet azimuth and 1.22 mrad in facet elevation.

LIMITS TO CANTING ANGLE ESTIMATIONS

One of the primary goals of this work has been to develop a system to measure heliostat canting errors to < 0.25 mrad accuracy. The canting angle calculations are only as good as the accuracy of the plane fit. We know that, in fact, the facets do have a very slight parabolic shape. We made the planar assumption for ease in computing, as well as assuming the center of the parabola is in the center of the mirror, limiting the bias in the normal of the plane fit. We looked at several factors. The first is the effect of the point density, or number of points on the facet. We simulated LiDAR scans of facets at known position and angles relative to the simulated sensor, and varied the point density and range noise. Comparisons are between the input angles and calculated angles. We found that, as expected, the more points on the plane, the lower the standard deviation. Assuming the range noise to be ± 0.002 mm (the declared noise

level of the scanner used), we averaged a thousand simulations at 2mm noise and found the standard deviation for point counts between 100 and 100,000. Figure 15 shows this data in a chart. The X axis is the number of points on the facet, and the Y axis is the standard deviation of the normal expressed as the azimuth angle. The blue plot are the values calculated. The red plot is the normalized $\frac{1}{sqrt(N)}$ showing the error value does indeed follow the rule of error reduction with increased points to analyze. Past a thousand points (0.048 mrad RMS), these numbers are significantly below the 0.25 mrad target.

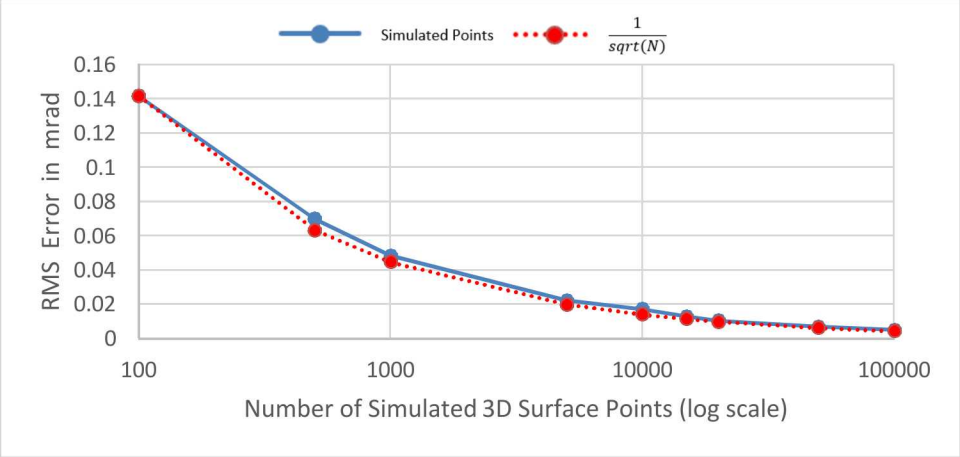

Figure 15. Plot of RMS error versus number of scan points on the facet.

A second factor we considered here was the effect of the angle of the facet to the scanner. It was thought the larger the angle, the greater the error. The simulation testing, at straight-on to 60 degrees off-axis to the sensor showed no noticeable difference in error, showing similar standard deviation errors as the previous test; well below the target goal. While this is optimistic in terms of how the heliostat can be scanned in the field, we still assume large off-angle scanning will have a detrimental effect on accuracy. Most surfaces will have a reduction in laser intensity relative to the incident angle with the scan beam, The lower the intensity, the greater the range error. The position of the scanner relative to the heliostat will have a direct relation to this incident angle. When the scanner is close to the heliostat, this angle to the lower facets versus upper facets can vary significantly. We have not yet verified this effect in the field.

CONCLUSIONS

This project considered the use of processed 3D point-cloud LiDAR scans of heliostats to calculate in-situ measurements of canting angles in the field. We have shown that LiDAR scanning is possible for valid data collection to measure heliostat facet canting angles, demonstrating this process in over two hundred field scans. We have noted the effect of facet soiling in the scanning process and have workable solutions for mirrors that are too clean. We have addressed the possibility to use either the front or back side of the heliostat for this process; however, where possible, the front side is recommended, primarily because it is unencumbered by support structures, and some heliostat designs do not expose the back-side mirror surface. We have addressed the effect of measurement noise in the calculations of plane fitting accuracy. We were able to automate the entire remote scanning and processing from a laptop computer which can complete the entire process in less than 5 minutes per heliostat. Based on the heliostats we have tested, and the repeatability studies conducted, we believe we have achieved the 0.25 mrad error accuracy requirements given at the start of this project.

FUTURE WORK

We initially hoped to tackle the tracking error problem by using the position data available in the scan, such as the base of the heliostat, and match it with real GPS locations. We were not at all accurate enough in our initial attempts. We assume this is because the available GPS data of heliostat positioning was itself not accurate enough to reach the desired levels of 0.5 mrad error. This needs further study to see if this, or some other method, can use readily available localization information to accomplish this task.

We do know this method is very amenable to data collection at night, or when the sun is not shining or the heliostats are otherwise inoperable. LiDAR scanners work even better without ambient light.

Potential for Autonomous Data Collection

It is wholly possible to mount the scanner and computer on a mobile platform and automate the entire heliostat scan process. The mobile platform would drive to a designated spot in front of each heliostat. This is very doable with path planning and collision avoidance onboard the robot to avoid driving issues. The platform would then initiate the scan, process the data, and move to the next heliostat. Some coordination with the field operation to place the heliostats in an acceptable position would also be needed. LiDAR scanners have already been deployed on commercial ground and air vehicles. Figure 16. FARO Trek; a LiDAR scanner on a mobile platform. shows a recently available commercial product from FARO Technologies called Trek [7]. This places a FARO scanner, like the one we used for this project, mounted on the back of SPOT, a robotic platform from Boston Dynamics.

Figure 16. FARO Trek; a LiDAR scanner on a mobile platform.

ACKOWLEDGEMENTS

Sandia National Laboratories is a multimission laboratory managed and operated by National Technology & Engineering Solutions of Sandia, LLC, a wholly owned subsidiary of Honeywell International Inc., for the U.S. Department of Energy's National Nuclear Security Administration under contract DE-NA0003525. The authors would like to thank the DOE Solar Energy Technology Office for supporting this research.

REFERENCES

1. E. Sproul, K. Chavez, J. Yellowhair, Heliostat Focusing and Canting Enhancement Technique: An Optical Heliostat Alignment Tool for the National Solar Thermal Test Facility," ES2011-54268, *Proceedings of the ASME 2011 5th International Conference on Energy Sustainability*, Washington, D.C, Aug. 7-10.
2. K. Chavez, E. Sproul, J. Yellowhair, Heliostat Facet Focusing and Characterization using the Heliostat Focusing and Canting Enhancement Technique, *Proceedings of the ASME 2012 6th International Conference on Energy Sustainability*, San Diego, CA, July 23-26.
3. Yellowhair, P. A. Apostolopoulos, D. E. Small, D. Novick, M. Mann, Development of an Aerial System for Heliostat Canting Assessments, *Proceedings of SolarPACES 2020 Online Conference*, Sept. 28 – Oct. 2.
4. Faro Focus 3D Scanner Website, https://www.faro.com/products/construction-bim/faro-focus/
5. Bounding Box Algorithm, https://github.com/GeoDaCenter/geoda/blob/master/libgdiam/README
6. A. C. Moya, C. K. Ho, Modeling and Validation of Heliostat Deformation Due to Static Loading, Proceedings of the ASME 2011 5th International Conference on Energy Sustainability & 9th Fuel Cell Science, Engineering and Technology, August 7-10, 2011, Washington DC, USA
7. Faro Website, https:// www.faro.com/news/faro-launches-trek-the-automated-3d-laser-scanning-integration